Electrical spectroscopy of the spin-wave dispersion and bistability in gallium-doped yttrium iron garnet

Carmiggelt, Joris J.; Dreijer, Olaf C.; Dubs, Carsten; Surzhenko, Oleksii; Van Der Sar, Toeno

DOI
10.1063/5.0070796

Publication date
2021

Document Version
Accepted author manuscript

Published in
Applied Physics Letters

Electrical spectroscopy of the spin-wave dispersion and bistability in gallium-doped yttrium iron garnet

Joris J. Carmiggelt[1], Olaf C. Dreijer[1], Carsten Dubs[2], Oleksii Surzhenko[2], Toeno van der Sar[1*]

[1] Department of Quantum Nanoscience, Kavli Institute of Nanoscience, Delft University of Technology, Lorentzweg 1, 2628 CJ Delft, The Netherlands
[2] INNOVENT e.V. Technologieentwicklung, D-07745 Jena, Germany

* Corresponding author. E-mail: t.vandersar@tudelft.nl

Abstract

Yttrium iron garnet (YIG) is a magnetic insulator with record-low damping, allowing spin-wave transport over macroscopic distances. Doping YIG with gallium ions greatly reduces the demagnetizing field and introduces a perpendicular magnetic anisotropy, which leads to an isotropic spin-wave dispersion that facilitates spin-wave optics and spin-wave steering. Here, we characterize the dispersion of a gallium-doped YIG (Ga:YIG) thin film using electrical spectroscopy. We determine the magnetic anisotropy parameters and Gilbert damping from the frequency and linewidth of the ferromagnetic resonance (FMR). Next, we use propagating spin wave spectroscopy in the Damon-Eshbach configuration to detect the small spin-wave magnetic fields of this ultrathin weak magnet over a wide range of wavevectors, enabling the extraction of the exchange constant $\alpha_{\mathrm{ex}} = 1.3(2) \times 10^{-12}\ \mathrm{J/m}$. We observe foldover of the FMR with increasing drive power, leading to frequency shifts of the spin-wave modes and a bistable region in the spin-wave spectra. Our results shed light on isotropic spin-wave transport in Ga:YIG and highlight the potential of electrical spectroscopy to map out the dispersion and bistability of propagating spin waves in magnets with a low saturation magnetization.

Yttrium iron garnet (YIG) is a magnetic insulator that is famous for its low Gilbert damping and long-range spin-wave propagation.[1] At low bias fields the YIG magnetization is typically pushed in the plane by the demagnetizing field,[2] leading to an anisotropic spin-wave dispersion at microwave frequencies. For applications that rely on spin-wave optics and spin-wave steering an isotropic spin-wave dispersion is desirable,[3,4] which can be achieved by introducing gallium dopants in the YIG: The presence of the dopants reduces the saturation magnetization and thereby the demagnetizing field,[5] and induces a perpendicular magnetic anisotropy (PMA),[6,7] such that the magnetization points out-of-plane. Isotropic transport of forward-volume spin waves has been observed even at zero bias field,[8] opening the door for spin-wave logic devices.[9–11]

To harness isotropic spin waves it is essential to know the spin-wave dispersion, which is dominated by the exchange interaction for magnets with a low saturation magnetization.[12] Here, we use all-electrical spectroscopy of propagating spin waves[13–17] to characterize the spin-wave dispersion of a 45-nm-thick film of gallium-doped YIG (Ga:YIG). Rather than looking at the discrete mode numbers of perpendicular standing spin waves,[18] this method enables extracting the exchange constant by monitoring the spin-wave transmission for a continuously-tunable range of wavevectors. We show that this technique has sufficient sensitivity to characterize spin waves in nanometer-thick Ga:YIG films, where perpendicular modes may be challenging to detect due to their high frequencies and small mode overlap with the stripline drive field.

We extract the anisotropy parameters from the field dependence of the ferromagnetic resonance (FMR) frequency at different bias field orientations and find that the PMA is strong enough to lift the magnetization out of the plane. Next, we determine the damping of our film from the linewidth of the FMR and characterize the spin-wave dispersion from electrically-detected spin-wave spectra. We measure in the Damon-Eshbach configuration to boost the inductive coupling of the spin waves to the striplines,[19] allowing the extraction of the spin-wave group velocity over a wide range of wavevectors from which we determine the exchange constant. When increasing the microwave excitation power, we observe clear frequency shifts of the spin-wave modes. The shifts result from the foldover of the FMR, which we verify by comparing upward and downward frequency sweeps. These results benchmark propagating spin wave spectroscopy as an accessible tool to characterize the exchange constant and spin-wave bistability in technologically attractive thin-film magnetic insulators with low saturation magnetization and PMA.

We use liquid phase epitaxy to grow a 45-nm-thick film of Ga:YIG on an (111)-oriented gadolinium gallium garnet (GGG) substrate (supplementary material section 1). Using vibrating sample magnetometry (VSM) we determine the saturation magnetization $M_\mathrm{s} = 1.52(6) \times 10^4\ \mathrm{A/m}$ (Fig. 1(a), the number in parentheses denotes the 95% confidence interval), which is approximately an order of magnitude smaller than undoped YIG films of similar thicknesses.[20]

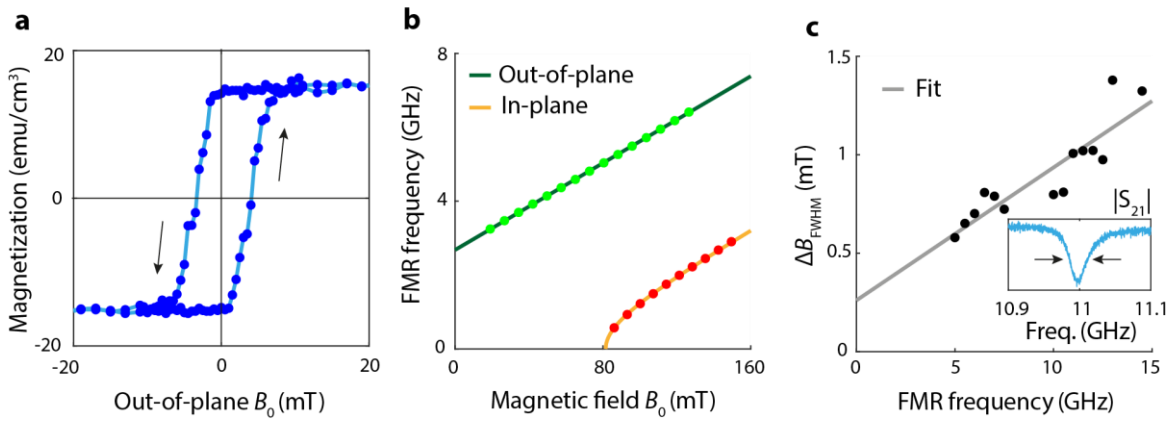

Figure 1: The saturation magnetization, magnetic anisotropies and Gilbert damping of Ga:YIG. (a) Hysteresis loop of the magnetization of a 45-nm-thick Ga:YIG film as a function of out-of-plane magnetic field B_0 measured using vibrating sample magnetometry and corrected for magnetic background. The arrows denote the sweep direction of the magnetic field. (b) FMR measurements using an out-of-plane (green) and in-plane (red) magnetic field B_0. From the fits of the FMR frequencies (solid lines) we determine the perpendicular and cubic anisotropy fields (see text). (c) Frequency dependence of the FMR linewidth. The data points are obtained from FMR absorption spectra at different in-plane magnetic fields (see the inset for an example measurement). We convert the absorption spectra to the magnetic field scale using equation 2 and fit them with a Lorentz function to extract the full-width at half-maximum (FWHM, ΔB_{FWHM}). From the linear fit (solid grey line) we extract the Gilbert damping $\alpha_{\mathrm{G}} = 1.0(3) \times 10^{-3}$.

In addition to PMA, Ga:YIG films also have a cubic magnetic anisotropy due to a cubic unit cell. We start by determining the cubic and perpendicular anisotropy fields from the ferromagnetic resonance (FMR) frequencies $\omega_{\mathrm{FMR}}/2\pi$ using an out-of-plane ($\perp$) and in-plane ($||$) magnetic bias field B_0. For (111)-oriented films the out-of-plane and in-plane Kittel relations are given by[20,21]

$$\omega_{\mathrm{FMR}(\perp)} = \gamma_{\perp}\left(B_0 - \mu_0 M_{\mathrm{s}} + \frac{2K_{2\perp}}{M_{\mathrm{s}}} - \frac{4K_4}{3M_{\mathrm{s}}}\right), \tag{1}$$

$$\omega_{\mathrm{FMR}(\|)} = \gamma_{\|}\sqrt{B_0(B_0 + \mu_0 M_{\mathrm{s}} - \frac{2K_{2\perp}}{M_{\mathrm{s}}} - \frac{K_4}{M_{\mathrm{s}}})}. \tag{2}$$

Here $\gamma_{\perp,||} = g_{\perp,||}\mu_{\mathrm{B}}/\hbar$ is the gyromagnetic ratio with $g_{\perp,||}$ the anisotropic g-factor, μ_{B} the Bohr magneton and $\hbar$ the reduced Planck constant, μ_0 is the magnetic permeability of free space, $K_{2\perp}$ is the uniaxial out-of-plane anisotropy (e.g. PMA) constant and K_4 the cubic anisotropy constant. During the in-plane FMR measurement we apply the magnetic field along the $[1\bar{1}0]$ crystallographic axis to minimize the out-of-plane component of the magnetization (supplementary material section 2). We neglect any uniaxial in-plane anisotropy as it is known to be small in YIG samples.[20]

By substituting the value of M_s that we obtained with VSM into equations 1 and 2, we can determine $K_{2\perp}$ and K_4 from the FMR frequencies (Fig. 1(b)).[22] From the fits (solid lines) we extract the uniaxial out-of-plane anisotropy field $2K_{2\perp}/M_s = 104.7(8)\ \mathrm{mT}$ and the cubic anisotropy field $2K_4/M_s = -8.2(5)\ \mathrm{mT}$ (supplementary material section 3). Undoped YIG films of similar thicknesses have comparable cubic anisotropy fields,[20] which agrees with previous work on micrometer-scale films showing that the cubic anisotropy of YIG does not depend on gallium concentration.[23] We determine the in-plane and out-of-plane g-factors to be $g_{\parallel} = 2.041(4)$ and $g_{\perp} = 2.101(3)$.[24]

We extract the Gilbert damping α_G of our film from the linewidth ΔB_{FWHM} of the FMR,[25] which is given by

$$\Delta B_{\mathrm{FWHM}} = \Delta B_0 + \frac{2\alpha_G}{\gamma_{||}}\omega_{\mathrm{FMR}(||)}. \quad (3)$$

Here ΔB_0 is the inhomogeneous broadening and the magnetic field is applied in the plane. By fitting the frequency dependence of the FMR linewidth we find $\alpha_G = 1.0(3) \times 10^{-3}$ (Fig. 1(c)), which is about three times larger than for bismuth-doped YIG films of similar thickness.[26,27]

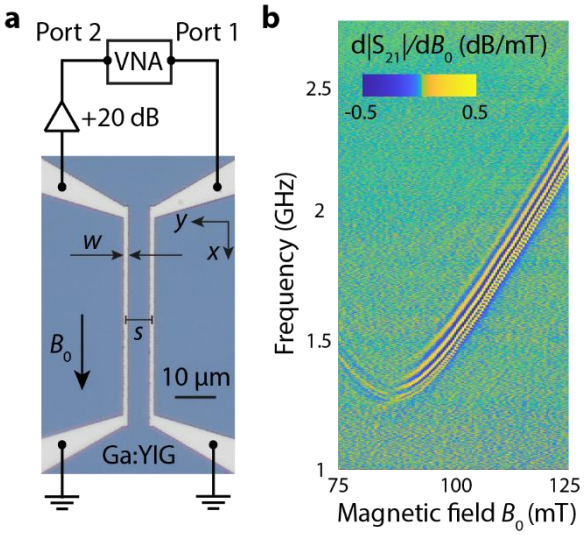

Figure 2: All-electrical propagating spin wave spectroscopy. (a) Optical micrograph of a Ga:YIG film with two gold striplines that are connected to the ports of a vector network analyser (VNA). Port 1 applies a microwave current (typical excitation power: $-35\ \mathrm{dBm}$) that induces a radio-frequency magnetic field B^{RF} at the injector stripline. This field excites propagating spin waves that couple inductively to the detector stripline at a distance s. The generated microwave current is amplified and detected at port 2. A static magnetic field B_0 is applied in the Damon-Eshbach configuration and is oriented such that the chirality of B^{RF} favours the excitation of spin waves propagating towards the detector stripline.[28] (b) Field-derivative of the microwave transmission $|S_{21}|$ between two striplines ($w = 1\ \mu\mathrm{m}$, $s = 6\ \mu\mathrm{m}$) as a function of B_0 and microwave frequency. The colormap is squeezed, such that also fringes corresponding to low-amplitude spin waves are visible. A masked background was subtracted to highlight the signal attributed to spin waves (supplementary material section 4).

We now use propagating spin wave spectroscopy to characterize the spin-wave dispersion in Ga:YIG. We measure the microwave transmission $|S_{21}|$ between two microstrips fabricated directly on the Ga:YIG as a function of static magnetic field B_0 and frequency f (Fig. 2(a)). The magnetic field is applied in the Damon-Eshbach geometry to maximize the inductive coupling between the spin waves and the striplines.[19] We measure a clear Damon-Eshbach spin-wave signal in the microwave transmission spectrum when B_0 overcomes the PMA and pushes the spins in the plane (Fig. 2(b), supplementary material section 4). The signal appears at a finite frequency, because the bias field B_0 is applied along the $[11\overline{2}]$ crystallographic axis with a finite out-of-plane angle of $\sim 1°$ (supplementary material section 2).

The fringes in the transmission spectra result from the interference between the spin waves and the microwave excitation field.[29,30] Each fringe indicates an extra spin-wavelength λ that fits between the striplines. We can thus use the fringes to determine the group velocity v_g of the spin waves via[14]

$$v_\mathrm{g} = \frac{\partial \omega_\mathrm{sw}}{\partial k} \approx \frac{2\pi\Delta f}{2\pi/s} = \Delta f s. \tag{4}$$

Here $\omega_\mathrm{sw} = 2\pi f$ and $k = 2\pi/\lambda$ are the spin wave's angular frequency and wavevector, Δf is the frequency difference between two consecutive maxima or minima of the fringes (Fig. 3(a)) and s is the center-to-center distance between both microstrips.

We extract the exchange constant of our Ga:YIG film by fitting the measured group velocity to an analytical expression derived from the spin-wave dispersion. The Damon-Eshbach spin-wave dispersion for magnetic thin films with cubic and perpendicular anisotropy is given by[21] (supplementary material section 5)

$$\omega_\mathrm{sw}(k) = \sqrt{\omega_B(\omega_B + \omega_M - \omega_K) + \frac{\omega_M t}{2}(\omega_M - \omega_K)k + \gamma_\parallel D(2\omega_B + \omega_M - \omega_K)k^2 + \gamma_\parallel^2 D^2 k^4}. \tag{5}$$

Here we defined for notational convenience $\omega_B = \gamma_\parallel B_0$, $\omega_M = \gamma_\parallel \mu_0 M_\mathrm{s}$ and $\omega_K = \gamma_\parallel(2K_{2\perp}/M_\mathrm{s} + K_4/M_\mathrm{s})$, t is the thickness of the film and $D = 2\alpha_\mathrm{ex}/M_\mathrm{s}$ is the spin stiffness, with α_ex the exchange constant. Differentiating with respect to k gives an analytical expression for the group velocity

$$v_\mathrm{g}(k) = \frac{1}{2\sqrt{\omega_\mathrm{sw}(k)}}\left(\frac{\omega_M t}{2}(\omega_M - \omega_K) + 2\gamma_\parallel D(2\omega_B + \omega_M - \omega_K)k + 4\gamma_\parallel^2 D^2 k^3\right). \tag{6}$$

Since we determined M_s and the anisotropy constants from the VSM and FMR measurements, the exchange constant is the only unknown variable in the dispersion. We determine the exchange constant from spin-wave spectra measured using two sets of striplines with different widths and line-to-line distances ($w = 1\ \mu\mathrm{m}$, $s = 6\ \mu\mathrm{m}$ and $w = 2.5\ \mu\mathrm{m}$, $s = 12.5\ \mu\mathrm{m}$) at the same static field (Fig. 3(a,b)). First we extract v_g as a function of frequency from the extrema in the spin-wave spectra using

equation 4 (Fig. 3(c)). By then fitting the measured $v_g(f)$ using equations 5 and 6 (solid line in Fig. 3(c)), we find $\alpha_{ex} = 1.3(2) \times 10^{-12}$ J/m and $B_0 = 117.5(3)$ mT (supplementary material section 3). The determined exchange constant is about 3 times smaller compared to undoped YIG,[18] which is in line with earlier observations of a decreasing exchange constant with increasing gallium concentration in micrometer-thick YIG films.[31] Simultaneously the spin stiffness is increased by about 3 times compared to undoped YIG[18] due to the strong reduction of the saturation magnetization. Using the extracted exchange constant and Gilbert damping, we calculate a decay length of ~ 30 μm for spin waves with a wavelength of 1 μm (supplementary material section 6).

The spin-wave excitation and detection efficiency depends on the absolute value of the Fourier amplitude of the radio-frequency magnetic field B^{RF} generated by a stripline, which oscillates in k with a period given by $\Delta k = 2\pi/w$ (Fig. 3(e)).[29,30] To verify that the spin waves we observe are efficiently excited and detected by our striplines, we substitute the extracted exchange constant into equation 5 and plot the spin-wave dispersion (Fig. 3(f)). For small wavevectors the dispersion decreases due to the PMA in the sample, until the exchange interaction becomes dominant and the dispersion starts increasing. The shaded areas correspond to the frequencies of the spin-wave fringes (Fig. 3(a,b)) and the dashed lines indicate the nodes in $|B^{RF}(k)|$ of both striplines (Fig. 3(d,e)). We conclude that the fringes in Fig. 3(a) correspond to spin waves excited by the first maximum of $|B^{RF}(k)|$ and that the fringes in Fig. 3(b) correspond to spin waves excited by the second maximum.

Surprisingly, we do not observe fringes in Fig. 3(b) corresponding to the first maximum of $|B^{RF}(k)|$, but rather see a dip in this frequency range (arrows in Fig. 3(b,f)). This can be understood by noting that the average frequency difference between the fringes would be smaller than the spin-wave linewidth (supplementary material section 7). Low-amplitude fringes corresponding to small-wavelength spin waves excited by the second k-space maximum of the 1-μm-wide stripline are also visible (Fig. 2(b), supplementary material section 8). These results demonstrate that the spin-wave dispersion in weak magnets can be reliably extracted using propagating spin wave spectroscopy by combining measurements on striplines with different widths and spacings.

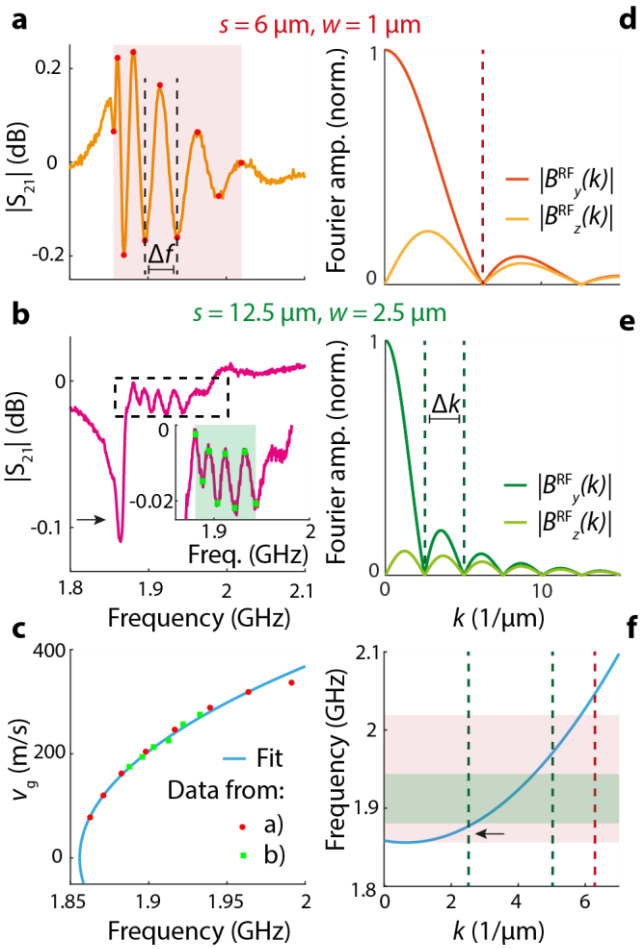

Figure 3: Extracting the exchange constant from spin-wave transmission spectra. (a,b) Background-subtracted linetraces of $|S_{21}|$ for two sets of striplines ((a): $w = 1\ \mu\text{m}$, $s = 6\ \mu\text{m}$, (b): $w = 2.5\ \mu\text{m}$, $s = 12.5\ \mu\text{m}$, excitation power: $-35\ \text{dBm}$). The red circles (a) and green squares (inset of (b)) mark the extrema of the spin-wave fringes. (c) From the frequency difference between the extrema Δf we determine the group velocity v_g of the spin waves at the center frequency between the extrema. The blue line fits the data with an analytical expression for v_g, extracting the exchange constant $\alpha_{ex} = 1.3(2) \times 10^{-12}\ \text{J/m}$. (d,e) Normalized Fourier amplitude of the y and z components of the microwave excitation field B^{RF} for striplines with widths $w = 1\ \mu\text{m}$ (d) and $w = 2.5\ \mu\text{m}$ (e). (f) Reconstructed spin-wave dispersion based on the fit in (c). The shaded areas correspond to the frequencies of the extrema in (a,b). The dashed lines are the same as in (d,e) and indicate the nodes in $|B^{RF}(k)|$ of the striplines. Only spin waves that are efficiently excited and detected by the striplines are observed in (a,b).

When strongly driven to large amplitudes, the FMR behaves like a Duffing oscillator with a bistable response.[32] Such bistability could potentially be harnessed for microwave switching.[33] Foldover of the FMR and standing spin-wave modes has been studied for several decades,[32–34] but bistability of propagating spin waves was only observed before in active feedback rings,[35] spin-pumped systems[36] and magnonic ring resonators.[37] We show that we can characterize the bistability of propagating spin waves in Ga:YIG thin films using our spectroscopy technique.

When increasing the drive power we observe frequency shifts of the spin waves (Fig. 4(a)). These non-linear shifts result from the four-magnon self-interaction term in the spin-wave Hamiltonian. For an in-plane magnetized thin film, the shifts are given by[38]

$$\widetilde{\omega_k} = \omega_k + W_{kk,kk}|a_k|^2. \quad (7)$$

Here $\widetilde{\omega_k}$ (ω_k) is the non-linear (linear) spin-wave angular frequency, $W_{kk,kk}$ is the four-wave frequency-shift parameter and a_k is the spin-wave amplitude. In our case $W_{kk,kk}$ is positive as a result of the PMA in the sample, leading to positive frequency shifts of the spin-wave modes and the FMR (supplementary material section 9).

At increased microwave power P, we observe an abrupt transition in the spin-wave spectrum (Fig. 4(a)) at which the spin waves fall back to their unshifted low-power frequencies. We find that the transition frequency scales linearly with $P^{1/3}$ for both upward and downward frequency sweeps (Fig. 4(b,c), dashed lines) and that it is larger for the upward sweep. Such a $P^{1/3}$ scaling was previously observed for FMR foldover in permalloy, where it was attributed to a significant non-linear damping term in the Duffing oscillator equation used to model the resonance[32]. This model predicts that the FMR amplitude becomes bistable at large drive power (Fig. 4(d)) and abruptly switches between the high- and low-amplitude states at a transition frequency that scales with $P^{1/3}$ for both up- and downward frequency sweeps.

We extract the bistability region by subtracting the upward and downward frequency sweeps of Fig. 4(b,c) and plotting the result in Fig. 4(e). We further highlight the bistability by plotting linetraces of the up- and downward frequency sweeps at $P = 0\ \mathrm{dBm}$ (Fig. 4(f)). The foldover starts at a surprisingly low drive power of $\sim -30\ \mathrm{dBm}$, potentially caused by reduced spin-wave scattering[34] due to the low density of states associated with the increased spin stiffness and reduced saturation magnetization of our sample.

The observed frequency shifts provide an extra knob for tuning the dispersion of spin waves. They give rise to strong non-linear microwave transmission between the striplines as a function of excitation power, which may provide opportunities for neuromorphic computing devices that simulate the spiking of artificial neurons above a certain input threshold.[37,39]

In summary, we used propagating spin wave spectroscopy to characterize the spin-wave dispersion in a 45-nm-thick film of Ga:YIG. The gallium doping reduces the saturation magnetization of the YIG and introduces a small PMA that lifts the magnetization out of the plane and causes the dispersion to be dominated by the exchange constant. We extract the exchange constant by fitting the group velocity at different frequencies and demonstrate that the detected spin waves are efficiently excited by the excitation fields of the striplines. Finally, we observe pronounced power-dependent frequency shifts and bistability of the spin waves, resulting from the foldover of the FMR. Our results highlight the potential of all-electrical spectroscopy to shed light on the dispersion and nonlinear response of propagating spin waves in weakly-magnetic thin films.

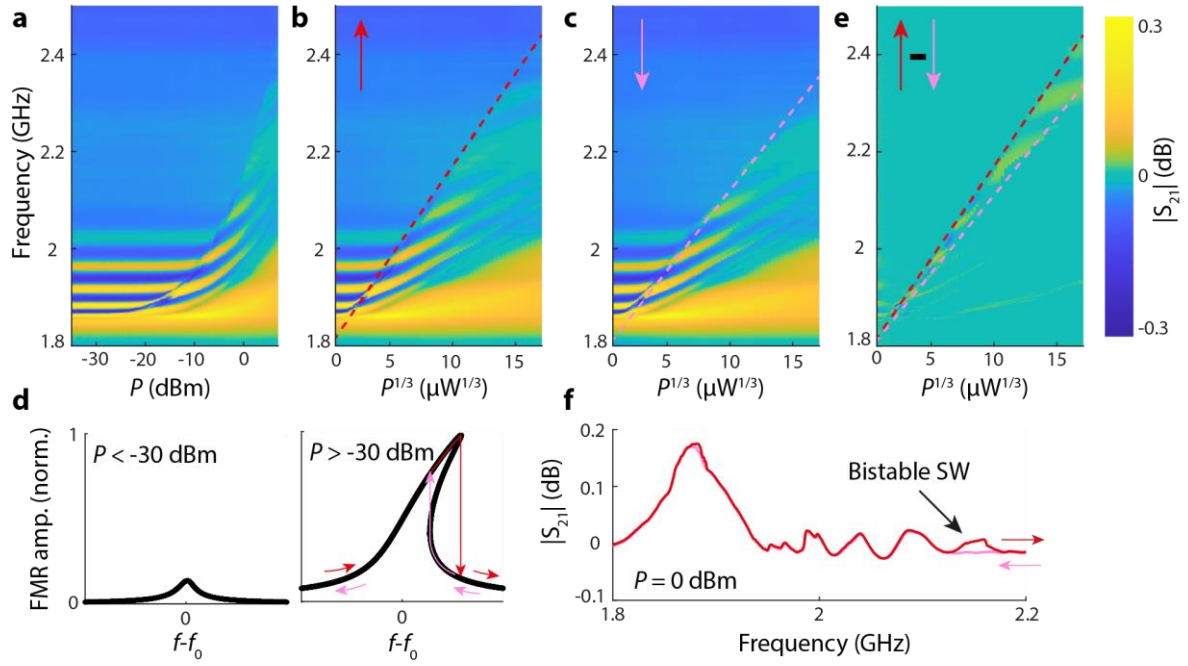

Figure 4: Observation of spin-wave frequency shifts and bistability. (a) Spin-wave spectra vs excitation power P for an upward frequency sweep ($w = 1\ \mu\mathrm{m}$, $s = 6\ \mu\mathrm{m}$). Low-frequency spin waves shift to higher frequencies when the microwave excitation power is increased. (b,c) Spin-wave spectra plotted against $P^{1/3}$ for an upward (b) and downward (c) frequency sweep. The transition frequency, indicated by the dashed lines, scales linearly with $P^{1/3}$. The frequency-sweep direction is indicated by arrows. (d) Sketch of the FMR amplitude vs drive frequency at low and high drive power assuming a non-linear (Duffing) oscillator response. As a result of the foldover at high drive power the amplitude becomes bistable. The amplitude jumps between the two stable branches at higher frequencies for upward frequency sweeps (red arrows) than for downward sweeps (pink arrows). This behaviour and its bistability is also observed in (b) and (c) for $P > -30\ \mathrm{dBm}$. (e) Difference spectra highlighting the bistability region, obtained by subtracting the spectra in (c) from those in (b). (f) Linetraces from panels (b) and (c) at $P = 0\ \mathrm{dBm}$, the black arrow indicates the bistability region. All dashed lines serve as a guide to the eye.

Supplementary material: See the supplementary material for methods, details on the data analysis and error estimations, additional measurements and calculations of the FMR frequency, spin-wave dispersion, decay length and non-linear frequency-shift parameter.

Author contributions: J.J.C. and T.v.d.S. conceived the experiment. J.J.C. and O.D. built the experimental setup, performed the experiments and analyzed the data. C.D. grew the Ga:YIG film and O.S. performed the VSM and FMR linewidth measurements. J.J.C. fabricated the striplines. J.J.C. and T.v.d.S. wrote the manuscript with contributions from all coauthors. T.v.d.S. supervised the project.

Acknowledgements: This work was supported by the Netherlands Organisation for Scientific Research (NWO/OCW), as part of the Frontiers of Nanoscience program and by the Deutsche Forschungsgemeinschaft (DFG, German Research Foundation) -271741898. The authors thank A.V. Chumak for reviewing the manuscript, A. Katan, E. Lesne for useful discussions and C.C. Pothoven for fabricating the magnet holders

used in the experimental setup. We also thank the staff of the TU Delft electronic support division and the Kavli Nanolab Delft for their support in soldering the printed circuit board and fabricating the microwave striplines.

Competing interests: The authors declare that they have no competing interests.

Data availability: All data contained in the figures are available in Zenodo.org at http://doi.org/10.5281/zenodo.5494466, reference number 40. Additional data related to this paper are available from the corresponding author upon reasonable request.

References

[1] A.A. Serga, A.V. Chumak, and B. Hillebrands, J. Phys. D. Appl. Phys. **43**, 264002 (2010).

[2] K.Y. Guslienko and A.N. Slavin, J. Magn. Magn. Mater. **323**, 2418 (2011).

[3] P. Pirro, V.I. Vasyuchka, A.A. Serga, and B. Hillebrands, Nat. Rev. Mater. (2021).

[4] A. Barman, G. Gubbiotti, S. Ladak, A.O. Adeyeye, M. Krawczyk, J. Gräfe, C. Adelmann, S. Cotofana, A. Naeemi, V.I. Vasyuchka, B. Hillebrands, S.A. Nikitov, H. Yu, D. Grundler, A. V Sadovnikov, A.A. Grachev, S.E. Sheshukova, J.-Y. Duquesne, M. Marangolo, G. Csaba, W. Porod, V.E. Demidov, S. Urazhdin, S.O. Demokritov, E. Albisetti, D. Petti, R. Bertacco, H. Schultheiss, V.V. Kruglyak, V.D. Poimanov, S. Sahoo, J. Sinha, H. Yang, M. Münzenberg, T. Moriyama, S. Mizukami, P. Landeros, R.A. Gallardo, G. Carlotti, J.-V. Kim, R.L. Stamps, R.E. Camley, B. Rana, Y. Otani, W. Yu, T. Yu, G.E.W. Bauer, C. Back, G.S. Uhrig, O.V. Dobrovolskiy, B. Budinska, H. Qin, S. van Dijken, A.V. Chumak, A. Khitun, D.E. Nikonov, I.A. Young, B.W. Zingsem, and M. Winklhofer, J. Phys. Condens. Matter **33**, 413001 (2021).

[5] P. Hansen, P. Röschmann, W. Tolksdorf, P. Hansen, P. Roschmann, and W. Tolksdorf, J. Appl. Phys. **45**, 2728 (1974).

[6] J.E. Mee, G.R. Pulliam, D.M. Heinz, J.M. Owens, and P.J. Besser, Appl. Phys. Lett. **18**, 60 (1971).

[7] D.M. Heinz, P.J. Besser, J.M. Owens, J.E. Mee, and G.R. Pulliam, J. Appl. Phys. **42**, 1243 (1971).

[8] A. Haldar, C. Tian, and A.O. Adeyeye, Sci. Adv. **3**, e1700638 (2017).

[9] S. Klingler, P. Pirro, T. Brächer, B. Leven, B. Hillebrands, and A.V. Chumak, Appl. Phys. Lett. **106**, 212406 (2015).

[10] N. Kanazawa, T. Goto, K. Sekiguchi, A.B. Granovsky, C.A. Ross, H. Takagi, Y. Nakamura, and M. Inoue, Sci. Rep. **6**, 30268 (2016).

[11] A.B. Ustinov, B.A. Kalinikos, and E. Lähderanta, J. Appl. Phys. **113**, 113904 (2013).

[12] B.A. Kalinikos and A.N. Slavin, J. Phys. C Solid State Phys. **19**, 7013 (1986).

[13] V. Vlaminck and M. Bailleul, Science **322**, 410 (2008).

[14] S. Neusser, G. Duerr, H.G. Bauer, S. Tacchi, M. Madami, G. Woltersdorf, G. Gubbiotti, C.H. Back, and D. Grundler, Phys. Rev. Lett. **105**, 1 (2010).

[15] J. Chen, T. Yu, C. Liu, T. Liu, M. Madami, K. Shen, J. Zhang, S. Tu, M.S. Alam, K.

Xia, M. Wu, G. Gubbiotti, Y.M. Blanter, G.E.W. Bauer, and H. Yu, Phys. Rev. B **100**, 104427 (2019).

[16] H. Qin, S.J. Hämäläinen, K. Arjas, J. Witteveen, and S. van Dijken, Phys. Rev. B **98**, 224422 (2018).

[17] J. Chen, C. Wang, C. Liu, S. Tu, L. Bi, and H. Yu, Appl. Phys. Lett. **114**, 212401 (2019).

[18] S. Klingler, A.V. Chumak, T. Mewes, B. Khodadadi, C. Mewes, C. Dubs, O. Surzhenko, B. Hillebrands, and A. Conca, J. Phys. D. Appl. Phys. **48**, 015001 (2015).

[19] U.K. Bhaskar, G. Talmelli, F. Ciubotaru, C. Adelmann, and T. Devolder, J. Appl. Phys. **127**, 33902 (2020).

[20] C. Dubs, O. Surzhenko, R. Thomas, J. Osten, T. Schneider, K. Lenz, J. Grenzer, R. Hübner, and E. Wendler, Phys. Rev. Mater. **4**, 024416 (2020).

[21] B.A. Kalinikos, M.P. Kostylev, N.V. Kozhus, and A.N. Slavin, J. Phys. Condens. Matter **2**, 9861 (1990).

[22] S.A. Manuilov, S.I. Khartsev, and A.M. Grishin, J. Appl. Phys. **106**, 123917 (2009).

[23] V.B. Bobkov, I.V. Zavislyak, and V.F. Romanyuk, J. Commun. Technol. Electron. **48**, 196 (2003).

[24] M. Farle, Reports Prog. Phys. **61**, 755 (1998).

[25] C. Dubs, O. Surzhenko, R. Linke, A. Danilewsky, U. Brückner, and J. Dellith, J. Phys. D. Appl. Phys. **50**, 204005 (2017).

[26] L. Soumah, N. Beaulieu, L. Qassym, C. Carrétéro, E. Jacquet, R. Lebourgeois, J. Ben Youssef, P. Bortolotti, V. Cros, and A. Anane, Nat. Commun. **9**, 3355 (2018).

[27] M. Evelt, L. Soumah, A.B. Rinkevich, S.O. Demokritov, A. Anane, V. Cros, J. Ben Youssef, G. de Loubens, O. Klein, P. Bortolotti, and V.E. Demidov, Phys. Rev. Appl. **10**, 041002 (2018).

[28] T. Yu, Y.M. Blanter, and G.E.W. Bauer, Phys. Rev. Lett. **123**, 247202 (2019).

[29] F. Ciubotaru, T. Devolder, M. Manfrini, C. Adelmann, and I.P. Radu, Appl. Phys. Lett. **109**, 012403 (2016).

[30] I. Bertelli, J.J. Carmiggelt, T. Yu, B.G. Simon, C.C. Pothoven, G.E.W. Bauer, Y.M. Blanter, J. Aarts, and T. van der Sar, Sci. Adv. **6**, eabd3556 (2020).

[31] J.W. Boyle, J.G. Booth, A.D. Boardman, I. Zavislyak, V. Bobkov, and V. Romanyuk, Le J. Phys. IV **07**, C1 (1997).

[32] Y.S. Gui, A. Wirthmann, and C.-M. Hu, Phys. Rev. B **80**, 184422 (2009).

[33] Y.K. Fetisov, C.E. Patton, and V.T. Synogach, IEEE Trans. Magn. **35**, 4511 (1999).

[34] Y. Li, V.V. Naletov, O. Klein, J.L. Prieto, M. Muñoz, V. Cros, P. Bortolotti, A. Anane, C. Serpico, and G. de Loubens, Phys. Rev. X **9**, 041036 (2019).

[35] P.A.P. Janantha, B. Kalinikos, and M. Wu, Phys. Rev. B **95**, 064422 (2017).

[36] K. Ando and E. Saitoh, Phys. Rev. Lett. **109**, 26602 (2012).

[37] Q. Wang, A. Hamadeh, R. Verba, V. Lomakin, M. Mohseni, B. Hillebrands, A.V. Chumak, and P. Pirro, Npj Comput. Mater. **6**, 192 (2020).

[38] P. Krivosik and C.E. Patton, Phys. Rev. B **82**, 184428 (2010).

[39] J. Feldmann, N. Youngblood, C.D. Wright, H. Bhaskaran, and W.H.P. Pernice, Nature **569**, 208 (2019).

[40] J.J. Carmiggelt, O.C. Dreijer, C. Dubs, O. Surzhenko, and T. van der Sar (2021). "Electrical spectroscopy of the spin-wave dispersion and bistability in gallium-doped yttrium iron garnet," Zenodo. http://dx.doi.org/10.5281/zenodo.5494466